International Journal Of
Industrial Electronics Control and Optimization
Print ISSN: 3517-2645
Online ISSN: 3568-2645
Homepage: https://ieco.usb.ac.ir/

An Adaptive Robust Square Root Unscented Kalman Filter for State of Charge Estimation for Lithium-ion Batteries

Ramazan Havangi[1]| Fatemeh Karimi[2]

Faculty of Electrical Engineering and Computer, University of Birjand, Birjand, Iran.[1,2]

Corresponding author's email: Havangi@Birjand.ac.ir

Article Info

Article type:
Research Article

Article history:
Received: **********
Received in revised form: **********
Accepted: **********
Published online: **********

Keywords:
State of charge, adaptive robust square root unscented Kalman filter, lithium-ion batteries.

ABSTRACT

Accurate estimation of the State of Charge (SOC) is essential for effective Battery Management Systems (BMS), as it directly affects the performance, safety, and lifespan of battery-powered devices. However, precise SOC estimation remains challenging due to the nonlinear dynamics of batteries and unpredictable process and measurement noise. This paper proposes a novel hybrid approach that combines an Adaptive Robust Square Root Unscented Kalman Filter (ARSRUKF) with Recursive Least Squares (RLS) to improve the accuracy and robustness of SOC estimation. The ARSRUKF enhances numerical stability by maintaining the semi-positive definiteness of covariance matrices and enables direct computation of their square roots, which improves both symmetry and computational efficiency. Unlike conventional filters such as the Extended Kalman Filter (EKF) and Unscented Kalman Filter (UKF), the ARSRUKF does not require prior knowledge of noise statistics, making it suitable for real-world applications with unknown or non-Gaussian noise. To further enhance filter performance, an Adaptive Neuro-Fuzzy Inference System (ANFIS) is integrated for real-time adjustment of noise covariances, allowing dynamic tuning of filter parameters based on system behavior. Experimental results under diverse operating conditions, including temperature fluctuations and varying noise levels, demonstrate that the proposed method consistently outperforms EKF and UKF. The presented framework offers a robust and accurate solution for SOC estimation, with broad applicability in electric vehicles, renewable energy storage systems, and portable electronic devices.

I. Introduction

As the global concerns regarding energy consumption and environmental sustainability intensify, the need for cleaner, more efficient technologies has never been greater. The electric vehicle (EV) industry has emerged as a key player in addressing these concerns, experiencing substantial growth in recent years. The transition from traditional internal combustion engine vehicles to electric-powered alternatives is seen as a significant step toward reducing carbon emissions and minimizing dependence on fossil fuels. Central to the success and performance of electric vehicles is the battery technology employed, with lithium-ion batteries being the preferred choice in most applications. These batteries offer a combination of high energy density, long cycle life, and a relatively low self-discharge rate, making them ideal for storing and supplying energy in EVs as well as renewable energy applications, such as solar and wind power storage [1].

The integration of lithium-ion batteries into electric vehicles necessitates the development of advanced Battery Management Systems (BMS) to monitor and optimize battery performance. The BMS plays a critical role in ensuring the safe and efficient operation of the battery by continuously monitoring key parameters such as voltage, current, and temperature. In addition, it estimates the SOC, which represents the remaining energy capacity of the battery [2]. Accurate SOC estimation is essential for maintaining battery operation within safe limits and for preventing conditions such as overcharging or deep discharging-both of which can significantly degrade battery lifespan. Moreover, reliable SOC estimation contributes to more effective energy management, thereby enhancing the

driving range and overall efficiency of electric vehicles [3]. In addition to estimation algorithms, several recent studies have explored robust control strategies at the power electronics level. For example, [2] presents an improved sliding mode controller for EV battery chargers designed to enhance voltage stability under input voltage fluctuations. While this approach effectively improves robustness at the power interface level, it does not address the challenges of internal battery state estimation. In contrast, the present study introduces an integrated filtering framework—ARSRUKF combined with RLS and ANFIS—that enhances the accuracy and robustness of SOC estimation under uncertain, nonlinear, and dynamic conditions. This methodology complements control-layer solutions by specifically targeting the estimation layer within battery management systems.

Over the years, various methods have been proposed for SOC estimation, each with its own strengths and limitations. These methods can generally be classified into three main categories: open-loop methods, model-free methods, and model-based methods [4-6]. Open-loop methods, such as ampere-hour (Ah) counting and open-circuit voltage (OCV) measurement, are commonly employed due to their simplicity and ease of implementation. The Ah counting method estimates SOC by integrating charge and discharge currents over time. However, this method is highly prone to cumulative errors, which can substantially impair estimation accuracy-particularly when the initial SOC is imprecisely known or when current measurement errors occur [8–9]. In contrast, the OCV method estimates SOC based on the well-established correlation between SOC and the open-circuit voltage of the battery. Although the OCV method can yield accurate results under controlled conditions, it requires the battery to remain at rest for a sufficient period to allow voltage stabilization, thereby rendering it unsuitable for real-time applications [10].

Model-free methods, which include techniques such as neural networks and fuzzy logic, represent an alternative approach to SOC estimation. These methods do not rely on predefined battery models but instead use machine learning algorithms to map battery parameters, such as voltage and current, directly to SOC values [11-12]. While model-free methods can achieve high accuracy, they require large amounts of training data and exhibit high computational complexity, making real-time implementation more challenging.

In contrast, model-based methods leverage mathematical models to describe the dynamics of the battery and use filtering techniques to estimate SOC. Among these, the EKF has become one of the most widely used techniques for SOC estimation. The EKF approximates nonlinear battery dynamics using a first-order Taylor series expansion and the Jacobian matrix [13]. However, the need for linearization introduces errors that can reduce the accuracy of the SOC estimation. To address this, the UKF was introduced as an alternative. The UKF provides a higher-order approximation of the nonlinear system dynamics and does not require linearization, offering improved estimation accuracy over the EKF [14].

While model-based approaches, such as EKF and UKF, provide valuable benefits, they face significant challenges, particularly when it comes to the estimation of noise characteristics, such as process and measurement noise covariances. In practical applications, noise characteristics are often not well-defined and may vary dynamically due to changing environmental conditions-such as temperature fluctuations-or the gradual degradation of battery components over time. If inaccurate assumptions are made regarding noise statistics, the performance of the filtering algorithm may deteriorate, resulting in reduced estimation accuracy and potential filter divergence [17]. To overcome this challenge, the Adaptive Unscented Kalman Filter (AUKF) has been developed. The AUKF addresses time-varying noise by continuously updating the process and measurement noise covariance matrices, thereby improving estimation accuracy and enhancing the robustness and stability of the filter in dynamic conditions [18–19]. However, the AUKF introduces additional computational complexity, particularly due to the need to repeatedly calculate the square root of the error covariance matrix at each time step, which can be inefficient for real-time applications [20-21].

To overcome these challenges and provide a more efficient solution for SOC estimation, this paper proposes a novel approach that combines the Adaptive Robust Square Root Unscented Kalman Filter (ARSRUKF) with RLS to handle scenarios where prior knowledge of noise statistics is unavailable. The ARSRUKF directly propagates and updates the square root of the state covariance matrix in its Cholesky factored form, significantly reducing the computational complexity associated with traditional filtering methods while improving numerical stability and estimation performance. Additionally, to optimize the performance of the filter further, ANFIS is integrated into the system to fine-tune the parameters of the square root UKF (SRUKF). This integration allows the ARSRUKF to adapt to changing operating conditions and handle non-Gaussian noise more effectively, making it particularly suitable for real-world applications where the system uncertainties are minimal and dynamic.

The remainder of this paper is organized as follows: Section 2 presents the equivalent circuit model (ECM) of the battery, which is used for simulating battery behavior. Section 3 introduces the RLS method for battery parameter estimation, highlighting its relevance to accurate SOC estimation. Section 4 discusses the implementation of the ARSRUKF for SOC estimation, detailing the filtering and adaptation processes involved. Section 5 presents the

simulation and experimental results, comparing the performance of the proposed method with existing approaches. Finally, Section 6 concludes the paper, summarizing the key findings and suggesting directions for future research in SOC estimation and battery management systems.

II. Battery modeling

Lithium-ion battery modeling approaches can be broadly categorized into two main types: electrochemical models and equivalent circuit models (ECMs). Electrochemical models utilize nonlinear differential equations to characterize the intricate chemical and physical processes occurring within the battery. While these models offer a comprehensive and precise representation of battery behavior, their high computational complexity renders them unsuitable for real-time state-of-charge (SOC) estimation. Conversely, ECMs provide a more practical alternative by approximating battery dynamics through electrical components such as resistors, capacitors, and voltage sources[22-25]. These models require fewer parameters and do not explicitly account for complex internal electrochemical reactions, making them well-suited for implementation in BMS. Among various ECM structures, the second-order RC model has been widely recognized as a favorable trade-off between modeling accuracy and computational efficiency. Due to its capability to capture the battery's dynamic behavior while maintaining a manageable computational load, this model is chosen for simulating the electrical characteristics of the battery, as depicted in Fig. 1.

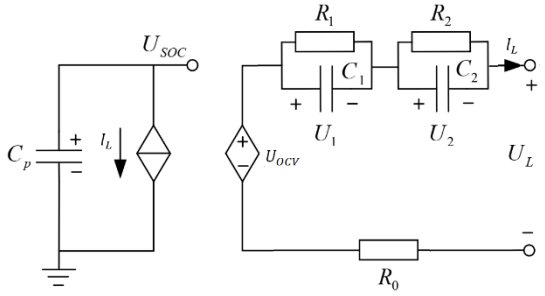

Fig 1. Second-order RC equivalent circuit model

The equivalent circuit model comprises a controlled voltage source (U_{SOC}) that models the nonlinear dependence of the battery's OCV on its SOC. A series resistance (R_0) is integrated to quantify the instantaneous ohmic losses during charge and discharge operations. To capture the transient dynamics of the battery, two distinct RC parallel networks (R_1, C_1, R_2 and C_2) are incorporated: the first network characterizes short-term polarization effects, while the second accounts for long-term diffusion processes. The voltage potentials across these RC elements, denoted as U_1, U_2 , describe the dynamic voltage deviations during operational cycles. Based on Kirchhoff's laws and transient circuit analysis, the system equations governing this model are expressed as follows [25]:

$$\dot{SOC} = -\frac{1}{Q_n} I_L$$
$$\dot{U_1} = -\frac{1}{R_1 C_1} U_1 + \frac{1}{C_1} \quad (1)$$
$$\dot{U_2} = -\frac{1}{R_2 C_2} U_2 + \frac{1}{C_2}$$

$$U_t = U_{OCV} - U_1 - U_2 - R_0 I_L \quad (2)$$

where Q_n is the nominal capacity of the battery in ampere-hours (Ah), U_{OCV} Open-Circuit Voltage $I_L$is load current, and U_t represents is the terminal voltage of the battery. Based on Equation (1), the state-space representation of the system in discrete time is given by [23]:

$$SOC(K+1) = SOC(K) - \frac{T}{Q_n} I_L(K)$$
$$U_1(K+1) = exp\left(-T/\tau_1\right) \times U_1(K) + \left[1 - exp\left(-T/\tau_1\right)\right] \times R_1 I_L(K) \quad (3)$$
$$U_2(K+1) = exp\left(-T/\tau_2\right) \times U_2(K) + \left[1 - exp\left(-T/\tau_2\right)\right] \times R_2 I_L(K)$$

$$U_t(k) = U_{OCV}(k) - U_1(k) - U_2(k) - R_0(k) I_L(K) \quad (4)$$

where T denotes the sampling period, which defines the discrete-time step used in the state-space representation of the battery model, $\tau_1 = R_1 C_1$ and $\tau_2 = R_2 C_2$are the time constants of the first and second RC branches, respectively.

III. Parameter identification

Parameter identification plays a crucial role in the process of battery modeling, ensuring that the battery model can accurately replicate the real-world behavior of the battery under various conditions. In this study, the least squares method is employed for parameter estimation, which is an efficient and widely used approach to minimize the difference between model outputs and observed data. The objective of this section is to estimate the parameters of the equivalent circuit model (ECM) that describe the behavior of the lithium-ion battery. In the equivalent circuit model, the battery voltage $U_t(s)$ in the Laplace domain is described as[22]:

$$U_t(s) = U_{OCV}(s) - (R_0 + \frac{R_1}{1 + R_1 C_1 s} + \frac{R_2}{1 + R_2 C_2 s}) I_L(s) \quad (5)$$

where s is the frequency operator,and $I_L(s)$represents the load current in the Laplace domain. Next, we define the transfer function $G(s)$ of the system as [25]:

$$G(s) = \frac{U_{OCV}(s) - U_t(s)}{I_L(s)} = R_0 + \frac{R_1}{1 + R_1 C_1 s} + \frac{R_2}{1 + R_2 C_2 s} \quad (6)$$

Defining the model parameters a and b as

$a = \tau_1\tau_2$, $b = \tau_1 + \tau_2$,

G(s) can be written as

$$G(s) = \frac{R_0 s^2 + \frac{1}{a}(bR_{0+}R_1\tau_2 + R_1\tau_2) + \frac{R_0 + R_1 + R_2}{a}}{s^2 + \frac{b}{a}s + \frac{1}{a}} \quad (7)$$

To discretize the system, we apply a bilinear transformation with the substitution $s = \frac{2}{T}\frac{1-z^{-1}}{1+z^{-1}}$ where T is the sampling period and z^{-1} represents the backward shift operator. This leads to the following discrete transfer function:

$$G(z^{-1}) = \frac{k_3 + k_4 z^{-1} + k_5 z^{-2}}{1 - k_1 z^{-1} - k_2 z^{-2}} \quad (8)$$

where $k_1, k_2, k_3, k_4$and k_5 are as follows:

$$k_1 = \frac{8a - T^2}{2bT + 4a + T^2}$$

$$k_2 = \frac{2bT - 4a - T^2}{2bTT + 4a + T^2}$$

$$k_3 = \frac{T^2(R_{0+}R_{1+}R_2) + 2TR_0 b + 4R_0 a + 2T(R_1\tau_2 + R_2\tau_1)}{2bT + 4a + T^2}$$

$$k_4 = \frac{2T^2(R_{0+}R_{1+}R_2) - 8R_0 a}{2bT + 4a + T^2}$$

$$k_5 = \frac{T^2(R_{0+}R_{1+}R_2) + 4R_0 a - 2R_0 T\tau_2 - 2T(R_1\tau_2 + R_2\tau_{1+}R_0\tau_1)}{2bT + 4a + T^2}$$

As a result, Equation (8) can be rewritten in the following difference equation form:

$$U_{OCV}(k) - U_t(k) = -k_1(U_{OCV}(k-1) - U_t(k-1)) - k_2(U_{OCV}(k-2) - U_t(k-2)) + k_3 I(k) + k_4 I(k-1) + k_5 I(k-2) \quad (9)$$

Defining $U_d(k)$ as:

$$U_d(k) = U_{OCV}(k) - U_t(k) \quad (10)$$

$$U_d(k) = U_{OCV}(k) - U_t(k)$$

Equation (6) can be written as

$$U_d(k) = k_1 U_d(k-1) + k_2 U_d(k-2) + k_3 I_L(k) + k_4 I_L(k-1) + k_5 I_L(k-2) \quad (11)$$

η(k)is set as the sampling error of the sensor at time k. Then, $U_d(k)$ can be written as:

$$U_d(k) = \emptyset(k)\theta(k) + \eta(k) \quad (12)$$

where the regressor vector $\emptyset(k)$ and parameter vector $\theta(k)$ are as follows:

$$\emptyset(k) = [U_d(k-1) \quad U_d(k-2) \quad I_L(k) \quad I_L(k-1) \quad I_L(k-2)]$$

$$\theta(k) = [k_1 \quad k_2 \quad k_3 \quad k_4 \quad k_5]$$

To estimate the parameters, the RLS method is applied. The recursive estimation equation is given by:

$$\hat{\theta}(k) = \hat{\theta}(k-1) + K(k)(y(k) - \emptyset(k)\hat{\theta}(k-1)) \quad (13)$$

$$\hat{\theta}(k) = \hat{\theta}(k-1) + K(k)(y(k) - \emptyset(k)\hat{\theta}(k-1))$$

where $\hat{\theta}(k)$ is the estimated parameter vector, and $y(k)$ is the observed output. The gain vector $K(k)$ is calculated as:

$$K(k) = P(k-1)\emptyset(k)^T(\lambda + \emptyset(k)P(k-1)\emptyset(k)^T)^{-1} \quad (14)$$

where $P(k-1)$ is the error covariance matrix and λ is a forgetting factor that determines how quickly past information is discarded. The updated error covariance matrix is given by:

$$P(k) = \frac{1}{\lambda}(P(k-1) - K(k)\emptyset(k)P(k-1)) \quad (15)$$

By using the recursive least squares method, the model parameters are iteratively adjusted to minimize the error between the predicted and observed voltage, thus improving the accuracy of the battery model over time. This approach provides an efficient way to estimate the parameters in real-time, making it suitable for use in Battery Management Systems.

IV. SOC estimation

To estimation SOC using ARSRUKF, the discrete state-space model of the battery is considered as follows:

$$x_k = f(x_{k-1}, U_k) + w_k \quad , \quad P(\omega_K) \sim N(0, Q_k)$$

$$z_k = h(x_k, U_k) + v_k \quad , \quad P(v_K) \sim N(0, R_k)$$

$$f(x_{k-1}, U_k) = \begin{bmatrix} e^{\frac{-T}{R_{1,k}C_{1,k}}} & 0 & 0 \\ 0 & e^{\frac{-T}{R_{2,k}C_{2,k}}} & 0 \\ 0 & 0 & 1 \end{bmatrix} x_{k-1} + \begin{bmatrix} R_{1,k}.\left(1 - e^{\frac{-T}{R_{1,k}C_{1,k}}}\right) \\ R_{2,k}.\left(1 - e^{\frac{-T}{R_{2,k}C_{2,k}}}\right) \\ \frac{-T}{C.3600} \end{bmatrix} I_{L,k} \quad (16)$$

$$h(x_k, U_k) = U_{OC,k} - U_{1,k} - U_{2,k} - R_0 I_{L,k}$$

A. H∞ extended filter

The H∞ filtering problem can be formulated based on game theory principles. In this approach, the performance measure is defined as follows [26]:

$$J=\frac{\sum_{k=0}^{k}\left\|x_k-\hat{x}_k\right\|_{S_k}^2}{\left\|x_0-\hat{x}_0\right\|_{P_0^{-1}}^2+\sum_{k=0}^{k}(\left\|w_k\right\|_{Q_k^{-1}}^2+\left\|v_k\right\|_{R_k^{-1}}^2)}<\gamma$$

where P_0^{-1} and S_k are weighting matrices, and $\hat{x}_k$ is determined such that $J<\gamma$. By selecting appropriate S_k, P_0, Q_k and R_k, prior knowledge about the influence of noise processes on the cost function can be incorporated into the estimation process. The H∞ extended filter is formulated as follows [26-27]:

$$\begin{aligned}&\hat{x}_k^- = f(x_{k-1},U_k)\\ &P_k^- = F_k P_{k-1} F_k^T + Q_k \ ,\ F_k=\frac{\partial f}{\partial x}\\ &K_k = P_k^- H_k^T (H_k P_k^- H_k^T + R_k)^{-1}\\ &\hat{x}_k = \hat{x}_k^- + K_k(z_k - h(\hat{x}_k^-))\end{aligned} \tag{17}$$

$$P_k = P_k^- - P_k^-\begin{bmatrix}H_k^T & I\end{bmatrix}R_{e,k}^{-1}\begin{bmatrix}H_k\\ I\end{bmatrix}P_k^- \tag{18}$$

$$H_k=\frac{\partial \mathrm{h}}{\partial \mathrm{x}}$$

where $R_{e,k}$ is as:

$$R_{e,k}=\begin{bmatrix}R_k & 0\\ 0 & -\gamma I\end{bmatrix}+\begin{bmatrix}H_k\\ I\end{bmatrix}P_k^-\begin{bmatrix}H_k^T & I\end{bmatrix}$$

B. SOC estimation using ARSRUKF

The SOC estimation using ARSRUKF is initialized by the matrix square root of the state covariance via a cholesky factorization as follows:

$$\begin{aligned}&\hat{x}_0 = E[x_0]\\ &S_0 = chol\{E[(x_0-\bar{x}_0)(x_0-\bar{x}_0)^T]\}\end{aligned} \tag{19}$$

A set of sigma points are calculated as:

$$\begin{aligned}&\chi_{k-1}^{[0]} = \hat{x}_{k-1}\\ &\chi_{k-1}^{[i]} = \hat{x}_{k-1}+\sqrt{n+\lambda}(S_{k-1})_i \qquad \text{i=1...n}\\ &\chi_{k-1}^{[i]} = \hat{x}_{k-1}-\sqrt{n+\lambda}(S_{k-1})_i \qquad \text{i=n+1...2n}\end{aligned} \tag{20}$$

where $\lambda=n(\alpha^2-1)$ and the constant α is small positive value. These sigma points are then propagated through the nonlinear process model, given by:

$$\chi_k^{[i]} = f(\chi_{k-1}^{[i]},U_k) \tag{21}$$

Subsequently, the transformed sigma points are used to estimate the state mean and square root of the covariance matrix:

$$\begin{aligned}&\hat{x}_k^- = \sum_{i=1}^{2n}\omega_i^{(m)}\chi_{k|k-1}^{[i]}\\ &S_k^- = qr(\sqrt{\omega_1^{(c)}}(\chi_k^{[1:2n]}-\hat{x}_k^-),\sqrt{Q_k})\\ &S_k^- = cholupdate(S_k^-,(\chi_k^{[0]}-\hat{x}_k^-),\omega_1^{(c)})\end{aligned} \tag{22}$$

where

$$\omega_0^{(c)}=\frac{\lambda}{n+\lambda}+(1-\alpha^2+\beta) \qquad \omega_0^{(m)}=\frac{\lambda}{n+\lambda}$$

$$\omega_i^{(m)}=\omega_i^{(c)}=\frac{\lambda}{2(n+\lambda)}$$

The square-root covariance matrix is updated using numerically stable orthogonal transformations. During the time update step, QR decomposition is employed to propagate the Cholesky factor of the covariance matrix, while rank-one updates are applied during the measurement update. This approach significantly enhances numerical stability by maintaining the positive definiteness of the covariance matrix and mitigating the accumulation of round-off errors that are often encountered in UKF. The transformed sigma points are then used to predict the measurements based on the measurement model, as follows:

$$\Im^{[i]} = h(\chi_k^{[i]},U_k)$$

The expected measurement $\hat{z}_k^-$ is as:

$$\hat{z}_k^- = \sum_{i=0}^{2n}\omega_i^{(m)}\Im^{[i]}$$

The cross-correlation covariance P_k^{xz} and the measurement covariance P_k^{zz} can be approximated by:

$$\begin{aligned}&P_k^{zz} \ @E[z_k-\hat{z}_k^-][z_k-\hat{z}_k^-]^T = H_k P_k H_k^T\\ &P_k^{xz} \ @E[x_k-\hat{x}_k][z_k-\hat{z}_k^-]^T = P_k H_k^T\end{aligned} \tag{23}$$

On the other hand, using the predicted sigma points, P_k^{xz} and P_k^{zz} also determines as follows:

$$\begin{aligned}&P_k^{xz} = \sum_{i=0}^{2n}\omega_i^{(c)}(\chi_k^{[i]}-\hat{x}_k)(\Im^{[i]}-\hat{z}_k^-)^T\\ &P_k^{zz} = \sum_{i=0}^{2n}\omega_i^{(c)}(\Im^{[i]}-\hat{z}_k^-)(\Im^{[i]}-\hat{z}_k^-)^T + R_k\end{aligned} \tag{24}$$

Using extended H_∞ filter, the state mean and square root of covariance are updated using the actual measurement

$$\hat{x}_k = \hat{x}_k + P_k^{xz}[R+P_k^{xz}]^{-1}(z_k-\hat{z}_k) \tag{25}$$

$$\begin{aligned}&S_k = chol(P_k)\\ &P_k = P_k^- -\\ &\begin{bmatrix}P_k^{xz} & P_k^-\end{bmatrix}\begin{bmatrix}R+P_k^{xz} & P_{k-1}^{xz\,T}\\ P_k^{xz} & -\gamma^2 I+P_k^-\end{bmatrix}^{-1}\begin{bmatrix}P_k^{xz} & P_k^-\end{bmatrix}^T\end{aligned} \tag{26}$$

To enhance the efficacy of the proposed methodology, the optimal selection of the weighting matrices $Q_k$and R_k is critical. This necessity arises from the asymptotic relationship between H∞ and H_2 filtering frameworks: as the attenuation factor λ approaches infinity, the H∞ filter converges to the extended H_2 filter (EKF) in behavior. Consequently, the weighting matrices $Q_k$and R_k in H∞ filtering—and by extension, in the Robust Square-Root Unscented Kalman Filter (RSRUKF)—fulfill analogous

roles to the process noise covariance matrix Q_k and measurement noise covariance matrix R_k in H_2-based filtering. Given this functional equivalence, adaptive estimation of $Q_k$and $R_k$represents a viable strategy to maintain filter robustness under dynamic operating conditions. A practical method for assessing the need for filter recalibration involves continuous observation of the residual signal, defined as the discrepancy between measured and predicted outputs. Deviations in residual statistics (e.g., magnitude or covariance) often indicate suboptimal tuning of $Q_k$and R_k necessitating real-time adjustments through adaptive algorithms. Such approaches ensure optimal noise suppression and state estimation accuracy, particularly in systems with time-varying noise characteristics or model uncertainties.

$$r_k = z_k - \hat{z}_k \tag{20}$$

Here, $\hat{z}_k$ denotes the *predicted measurement* at time step *k*, and z_k represents the *actual observed measurement*. When the filter operates under ideal conditions, the residual sequence r_k should exhibit properties of zero-mean white noise, indicating optimal noise suppression and unbiased estimation. To validate this behavior, the theoretical residual covariance P_k^{zz} (derived analytically in Equation 17) must align with the empirical residual covariance $\hat{C}_k$, computed from real-world data. The empirical covariance $\hat{C}_k$ can be estimated adaptively using a moving-average window of size *N*. This involves averaging the outer product of residuals over the most recent N_w time steps:

$$\hat{C}_k = \frac{1}{N} \sum_{i=k-N_w+1}^{k} (r_i^T r_i) \tag{21}$$

In this paper, ANFIS is employed to tune R_k and Q_k. The implemented ANFIS consists of a five-layer network, as illustrated in Fig. 2. The inputs to ANFIS are r_k and δr_k, where δr_k is defined as follows:

$$\delta r_k = r_k - r_{k-1}$$

The outputs are δR_k and δQ_k that employ to tune R_k and Q_k as follows:

$$Q_k = Q_k + \delta Q_k$$

$$R_k = R_k + \delta R_k$$

The ANFIS model comprises two inputs—innovation and its derivative—each represented by three Gaussian membership functions (Low, Medium, High), resulting in a total of nine fuzzy inference rules. The Gaussian membership functions corresponding to the input variables are shown in Fig. 3. A first-order Sugeno-type inference system is employed to perform the fuzzy reasoning. The ANFIS is trained online using a hybrid learning algorithm that combines least squares estimation for the consequent parameters with gradient descent for the optimization of membership function parameters. To maintain adaptability and numerical stability, training is conducted over a sliding window of recent data samples.

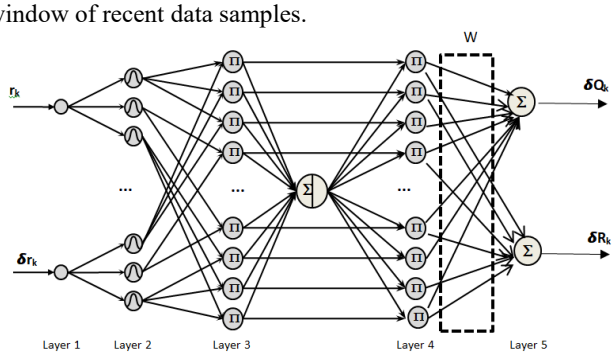

Fig.2. The ANFIS structure is used to tune R_k and Q_k

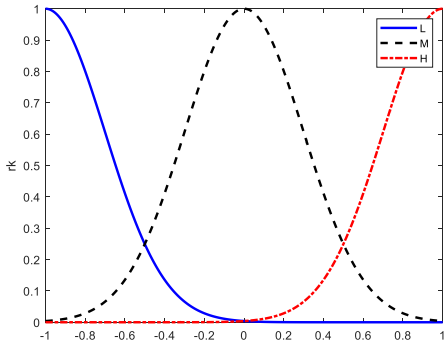

(a)

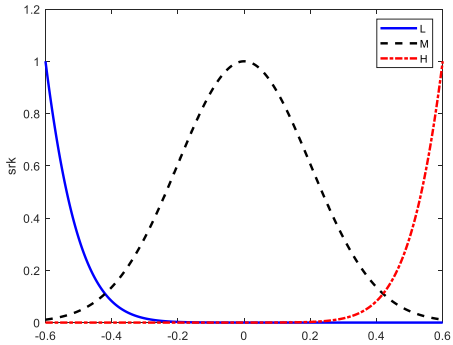

(b)

Fig.3. membership functions of ANFIS (a) r_k (b) δr_k

To describe the structure of ANFIS, assume that u_i^l and o_i^l represent the input and output of the i th node of the l th layer, respectively. The functioning of ANFIS is as follows:

Layer 1: Each node in this layer directly transmits its input values to the next layer

$$o_i^1 = u_i^1 \tag{27}$$

Layer2: In this layer, each node represents a membership function, and the output is computed as:

$$o_{ij}^{2} = \mu_{ij}(u^{2}) = \exp\left\{-\frac{(u_{ij}^{2} - m_{ij})^{2}}{(\delta_{ij})^{2}}\right\} \quad (28)$$

Where m_{ij} and δ_{ij} are the mean and width of the Gaussian membership function, respectively.

Layer3: Each neuron in this layer represents a fuzzy AND operation, which combines the incoming signals from Layer 2 by multiplying the membership function values. The output of each node is given by:

$$o_{l}^{3} = \prod_{i} u_{i}^{3} \quad (29)$$

Layer4: The node in this layer performs the normalization of firing strengths from layer 3,

$$o_{l}^{4} = \frac{u_{l}^{4}}{\sum_{l=1}^{9} u_{l}^{4}} \quad (30)$$

Layer5: This layer acts as a defuzzfier:

$$Output = \sum_{l=1}^{25} u_{l}^{5} w_{l} \quad (31)$$

The weighting of ANFIS is tuned using the steep descent algorithm such that the objective function E_k is minimized:

$$E_{k} = \frac{1}{2}(P_{k}^{zz} - \hat{C}_{k})^{2}$$

As a result, the weighting of ANFIS is updated as:

$$W_{k+1} = W_{k} - \eta \frac{\partial E_{k}}{\partial W_{k}}$$

Here η is learning rate of ANFIS. To maintain real-time model consistency, the RLS algorithm updates key battery parameters-such as internal resistance and RC pair values-at each time step using the most recent voltage and current measurements. These updated parameters are immediately integrated into the state-space model prior to ARSRUKF. This tightly coupled integration ensures synchronized model adaptation under dynamic operating conditions, including non-stationary behavior and rapid load variations. By continuously aligning the equivalent circuit model with real-time measurements, the RLS-enhanced framework ensures that both the prediction and correction phases of the ARSRUKF are based on the most accurate and up-to-date system representation. This real-time adaptability significantly improves estimation accuracy and filter robustness without relying on static model assumptions, enabling effective tracking of battery behavior in the presence of operating uncertainties.

V. Result

A test benchmark is performed to evaluate the proposed algorithms. The specifications of the test battery are summarized in Table I.

TABLE I CELL SPECIFICATION

Model	INR 18650-20R
Nominal Voltage(V)	3.6 V
Nominal Capacity (mAH)	2000mAh
Upper Cut-Off Voltage	4.2
Lower Cut-Off Voltage	2

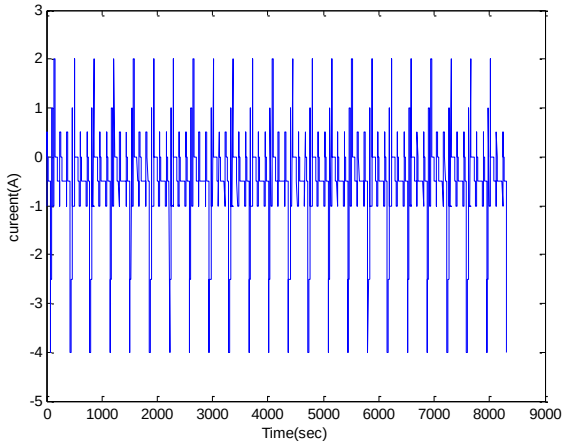

Fig. 4. Measured current

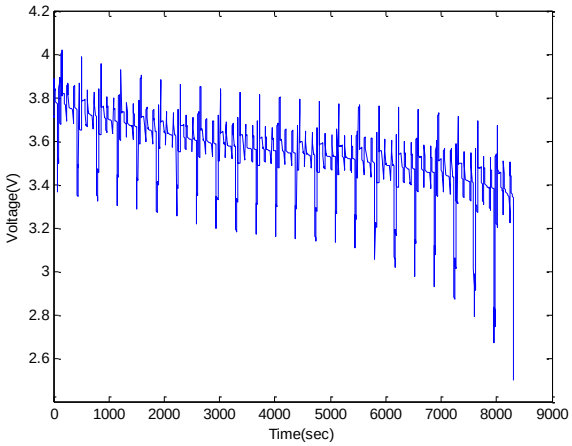

Fig.5. Measured voltage

A. Parameter identification

Accurate estimation of battery model parameters is essential for ensuring precise SOC estimation and improving the performance of BMS. To achieve this, a Dynamic Stress Test (DST) [28] is conducted, which is widely used for characterizing battery dynamics under realistic load conditions. The DST protocol involves applying a sequence of current pulses with varying amplitudes and durations while incorporating the effects of regenerative charging. This dynamic loading pattern is designed to capture the nonlinear behavior of the battery, including the impact of hysteresis, internal resistance variation, and transient response characteristics. The corresponding current profile

and terminal voltage response of the battery under DST conditions are depicted in Figs. 4 and 5. By analyzing the battery's voltage response to the applied current steps, key parameters such as internal resistance, open-circuit voltage, and equivalent circuit elements (e.g., resistance-capacitance pairs) can be extracted. Although the DST does not fully replicate real-world operating conditions—where temperature fluctuations, aging effects, and complex load variations exist—it provides a well-structured and repeatable framework for parameter estimation. The parameter identification results, presented in Fig.6, indicate that the estimated parameters converge effectively to their true values. This convergence confirms the accuracy and reliability of the identification process, demonstrating that the selected modeling approach effectively captures the battery's electrical characteristics. The results also highlight the robustness of the estimation algorithm in handling variations in operating conditions, which is crucial for enhancing battery state estimation and predictive modeling in practical applications.

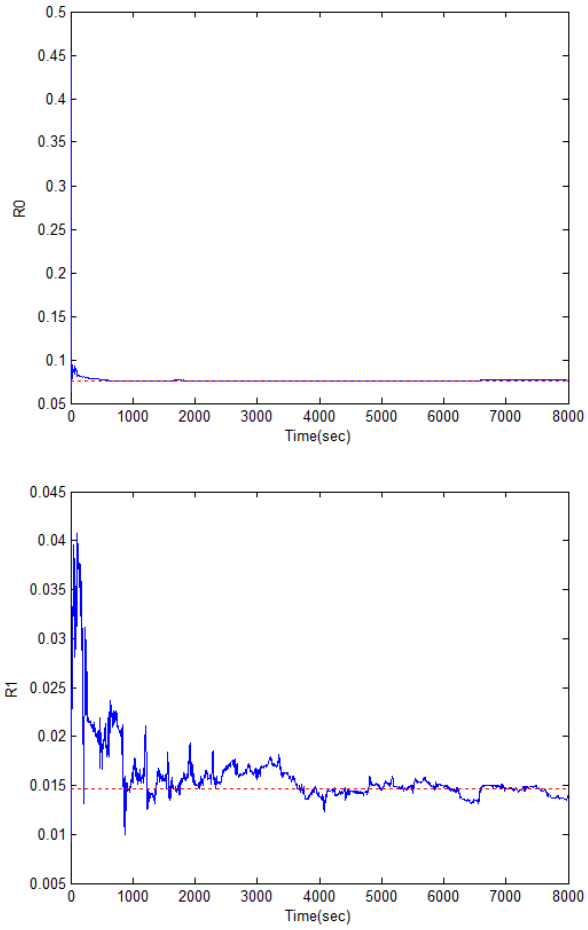

Fig.6. Battery parameter identification results

Before proceeding with SOC estimation, it is crucial to validate the accuracy of the battery model. To achieve this, a model verification test is performed using the Federal Urban Driving Schedule (FUDS) [29], which serves as a standard benchmark for evaluating model performance. Fig. 7(a) presents the battery terminal voltage along with its estimation error during the FUDS test. As illustrated in Fig. 7(b), the discrepancy between the estimated and measured

voltage remains minimal, confirming that the model provides a reliable representation of the battery's behavior.

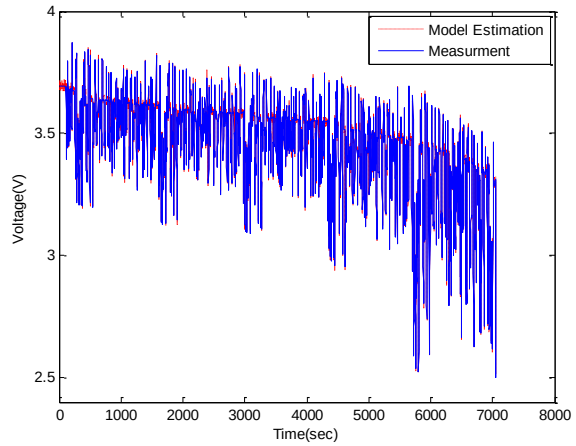

(a)

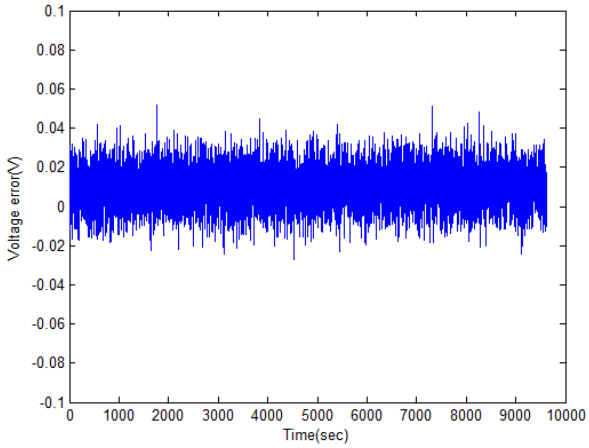

(b)

Fig.7. the results under FUDS: (a) Voltage comparison. (b) Voltage error.

B. SOC estimation

In this subsection, the accuracy and robustness of the proposed method are evaluated using standardized dynamic current profiles, including FUDS [29] and the US06 Highway Driving Schedule [30]. These profiles are more demanding than DST due to their highly variable charge and discharge rates, thereby offering a more rigorous assessment of estimation performance. The proposed method estimates SOC during both charging and discharging phases by incorporating bidirectional current flow into the state-space model. Specifically, the SOC update equation accounts for current polarity, with positive values indicating charging and negative values indicating discharging. To ensure accurate bidirectional behavior, model parameters were identified using RLS based on complete charge–discharge cycles. Experimental validation under the FUDS and US06 profiles—which include regenerative braking events—demonstrated robust SOC tracking performance. These results confirm the applicability of the proposed method in real-world battery management systems that require reliable SOC estimation under dynamic and bidirectional operating conditions. The corresponding current profiles used for testing are shown in Fig. 8.

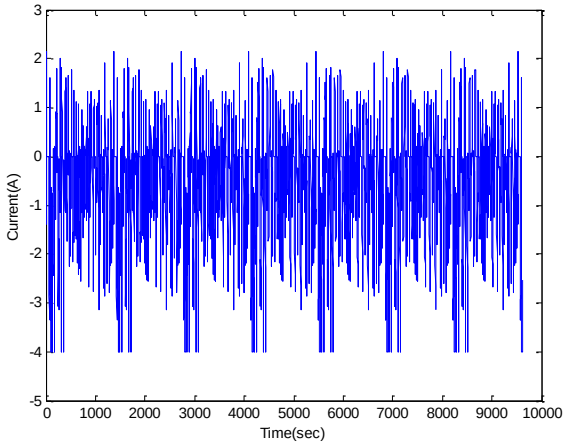

(a)

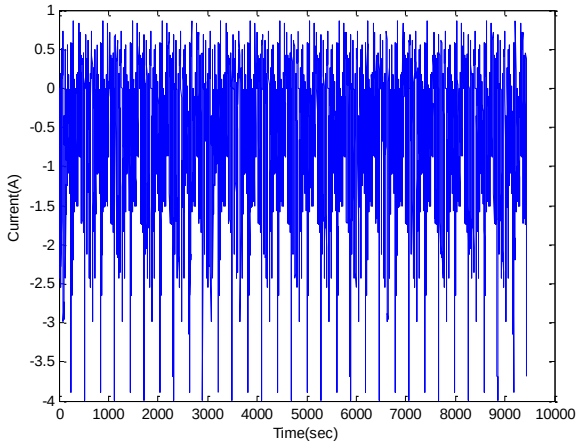

(b)

Fig.8. Battery test loading profiles: (a) Federal Urban Driving Schedule (FUDS) (c) US06 Highway Driving Schedule

First, the performance of the proposed method is evaluated and compared with existing approaches under the assumption that the statistical characteristics of noise are known a priori. To highlight proposed method advantages, the results are benchmarked against those obtained using UKF and EKF. Fig. 9 presents the SOC estimation results for the US06 and FUDS test profiles. Compared to the EKF and UKF, the SOC estimated by the proposed method exhibits a closer alignment with the actual SOC curves. Furthermore, the proposed method not only converges more accurately to the true SOC values but also maintains consistency in magnitude, demonstrating its superior accuracy and reliability in SOC estimation.

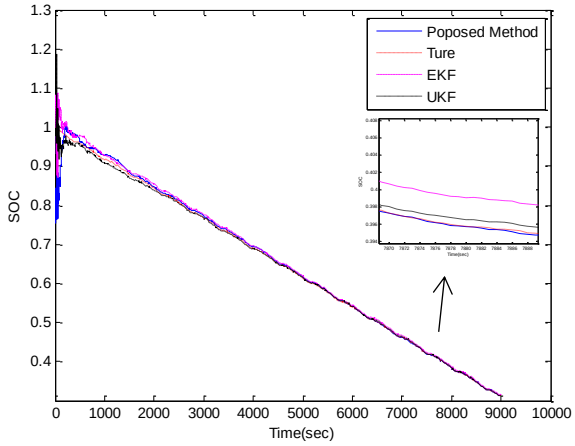

(a)

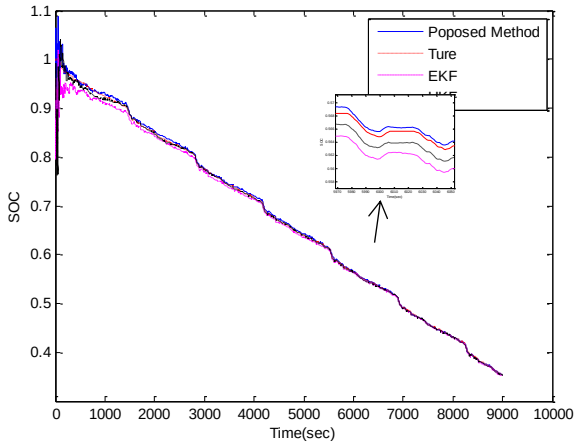

(b)

Fig.9. SOC estimation at 0 C (a) US06 (b) FUDS

TABLE II SENSITIVITY ANALYSIS OF ANFIS PARAMETERS ON SOC ESTIMATION PERFORMANCE

Parameter	Range	Observed Behavior	Optimal Value
Number of Membership Functions	2 – 4	<3 Underfitting; >3 negligible improvement, increased complexity	3
Learning Rate η	0.001 – 0.03	η > 0.02: minor oscillations η < 0.005: slow adaptation	0.01
Forgetting Factor λ	0.90 – 0.999	λ < 0.95 more adaptive, sensitive to noise λ > 0.995: sluggish adaptation	0.98
λ =0.94	-	Very fast adaptation, but noticeable increase in residual noise and RMSE spikes	-

The performance of SOC estimation using the proposed method is indeed affected by the choice of ANFIS parameters; however, the framework has been deliberately designed to minimize sensitivity and maintain robustness even in the presence of slight parameter mis-tuning. To assess this robustness, we performed a sensitivity analysis focusing on three key ANFIS parameters: the number of membership functions per input, the learning rate η, and the forgetting factor λ. The findings, summarized in the newly added Table II, demonstrate that using fewer than three membership functions leads to underfitting, while increasing the number beyond three results in negligible accuracy gains at the cost of increased computational complexity. Furthermore, the SOC estimation remains stable for learning rates within the range η∈[0.005,0.02]; higher values can introduce minor oscillations in the estimated covariance matrices. The forgetting factor also exhibits a wide robustness range, with stable behavior observed for λ∈[0.95,0.995. Although smaller λ values improve adaptability, they may also increase sensitivity to transient disturbances. Overall, the proposed method maintains reliable SOC estimation performance across a practical range of ANFIS parameter settings, underscoring the robustness of the proposed adaptive mechanism.

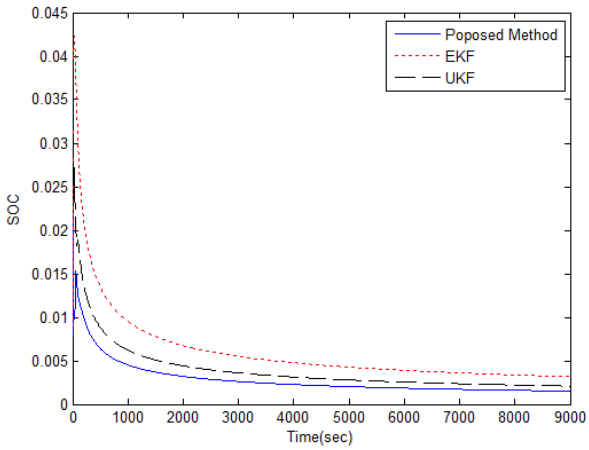

(a)

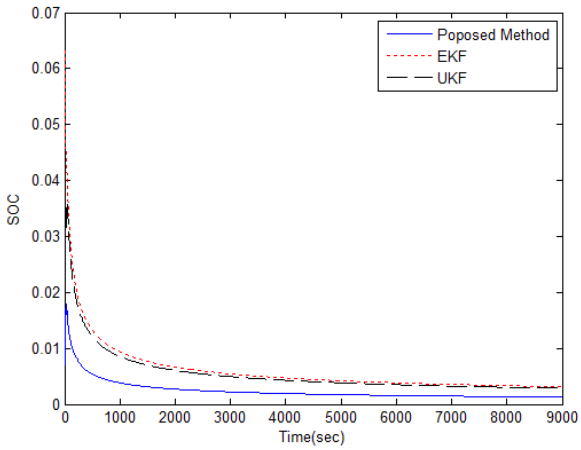

(b)

Fig.10. RMSE of SOC (a) US06 (b) FUDS

To further evaluate the estimation accuracy, the root mean square error (RMSE) is utilized as a performance metric. The RMSE is calculated over 50 Monte Carlo simulations for each estimation method. As shown in Fig. 10, the proposed method outperforms both the EKF and UKF in the FUDS

and US06 test scenarios. This improvement can be attributed to the proposed method's enhanced capability in accurately estimating both the mean and covariance, leading to more precise SOC predictions compared to the UKF and EKF.

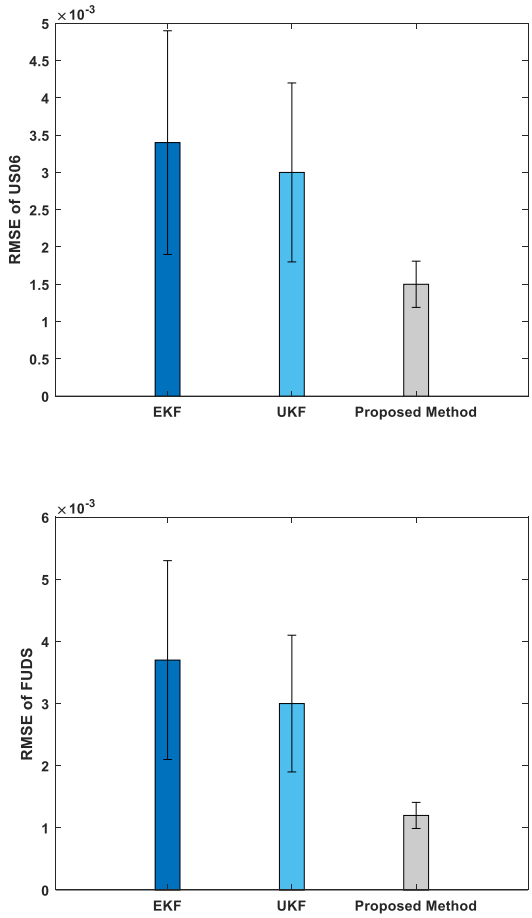

Fig.11. RMSE under known noise statistics

Fig.11 and Table III reports the mean RMSE, standard deviation, 95% confidence interval(CI) for pairwise comparisons. As shown, the proposed method achieves the lowest estimation error with significantly reduced variance. In the proposed method, several strategies have been employed to optimize performance on devices with limited computational resources. The use of a square-root formulation helps avoid matrix inversion, improving numerical stability and reducing computational complexity. Additionally, a compact ANFIS structure, consisting of only two inputs and nine fuzzy rules, minimizes the system's resource demands. The RLS algorithm is optimized with bounded updates to ensure efficient parameter estimation while keeping computational overhead low. To evaluate the computational efficiency of the proposed method, a detailed comparison with EKF and UKF implementations was conducted in Table IV. The findings under identical simulation settings MATLAB R2023a, Intel Core i7 @ 3.0 GHz, 16 GB RAM, single-threaded execution. As can be seen, the proposed method requires slightly higher runtime compared to EKF and UKF, but offers significantly improved accuracy and adaptive noise handling. This confirms that the added complexity due to ANFIS is marginal and feasible for real-time embedded implementation.

TABLE III RMSE UNDER KNOWN NOISE STATISTICS

Method	FUDS		US06	
	RMSE	95% CI	RMSE	95% CI
EKF	0.0037	0.0021–0.0053	0.0034	0.0019–0.0049
UKF	0.003	0.0019–0.0041	0.003	0.0018–0.0042
Proposed Method	0.0012	0.001–0.0014	0.0015	0.0012–0.0018

TABLE IV COMPUTATIONAL COMPLEXITY

Method	Computational Cost	Computational Complexity
EKF	0.15	$O(2n^3+m^3)$
UKF	0.42	$O((2n+1)n^2+n^3)$
Proposed Method	0.47	$O(n^3+p)O(n^3+p)$

Here, p denotes the set of ANFIS parameters, while n and m represent the number of state variables and measurement variables, respectively. In this study, we consider n = 3 and m = 1.

Next, the robustness of the proposed method is evaluated under scenarios where the measurement noise statistics are incorrectly assumed. In the proposed framework, real-time adaptive tuning is triggered when a significant discrepancy is detected between the empirical residual covariance—computed over a sliding window—and the theoretical innovation covariance. This strategy ensures that recalibration is activated only when persistent deviations are identified. To avoid overfitting to transient noise variations, windowed averaging is employed to smooth short-term fluctuations, and the ANFIS training is regularized using a forgetting factor ($\lambda = 0.98$) and a small learning rate ($\eta = 0.01$), enabling gradual and stable adaptation. The initial process and measurement noise covariance matrices (Q_0 and R_0) are selected based on empirical data and sensor specifications. Small diagonal values are used for Q_0 to account for model uncertainty, while R_0 is initialized based on nominal sensor noise levels. Importantly, the adaptive mechanism of the filter—driven by innovation-based statistics and ANFIS tuning—progressively refines these covariance matrices during operation. As a result, the long-term accuracy of SOC estimation remains robust to the initial selection of Q_0 and R_0.

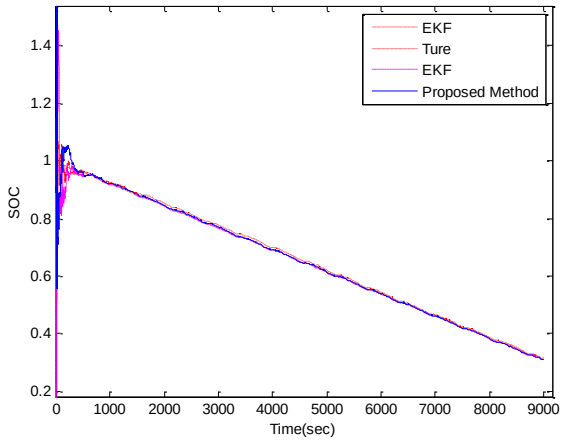

(a)

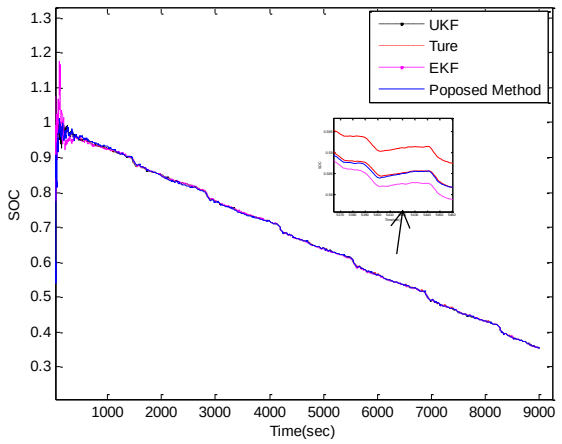

(b)

Fig.12. SOC estimation at 0 C (a) US06 (b) FUDS

Figs.11–12 present a comparative analysis of the proposed method against alternative approaches. The results indicate that the proposed method achieves superior accuracy compared to the EKF and UKF. Specifically, the SOC estimation results in Fig. 11 demonstrate that the proposed method rapidly converges to the actual SOC, highlighting its robustness even in the presence of unknown noise statistics. Furthermore, as shown in Figs. 11 and 13, the performance of the proposed method remains nearly unaffected compared to the previous case, whereas the performance of EKF and UKF degrades significantly. This resilience stems from the fact that the proposed approach does not rely on prior knowledge of noise statistics; instead, it operates under the assumption that the noise energy is bounded within a certain range. Additionally, the proposed method adaptively adjusts the process and measurement noise covariances, further enhancing its robustness.

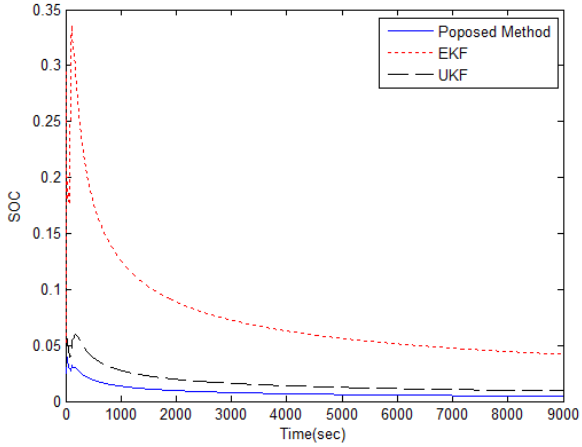

(a)

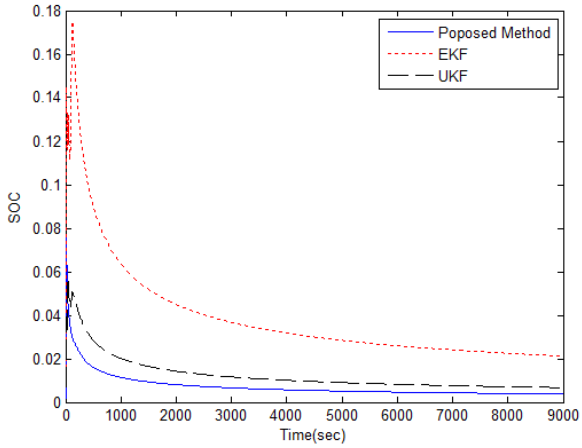

(b)

Fig.13. RMSE of SOC (a) US06 (b) FUDS

TABLE V RMSE UNDER UNKNOWN NOISE STATISTICS

Method	FUDS		US06	
	RMSE	95% CI	RMSE	95% CI
EKF	0.049	0.012-0.038	0.05	0.02-0.08
UKF	0.011	0.004-0.014	0.01	0.005-0.015
Proposed Method	0.003	0.0016-0.0026	0.003	0.0024-0.0036

To further demonstrate the advantages of the proposed approach over EKF and UKF, a quantitative comparison is conducted under identical simulation conditions. Fig. 12 illustrates the RMSE trajectories of SOC estimation over time, while Fig.14 the mean RMSE, standard deviation, 95% confidence interval for pairwise comparisons. Figs.13-14 and Table V present the RMSE results over 50 Monte Carlo simulations, confirming that the proposed method

consistently outperforms the EKF and UKF by achieving more accurate mean and covariance estimates.

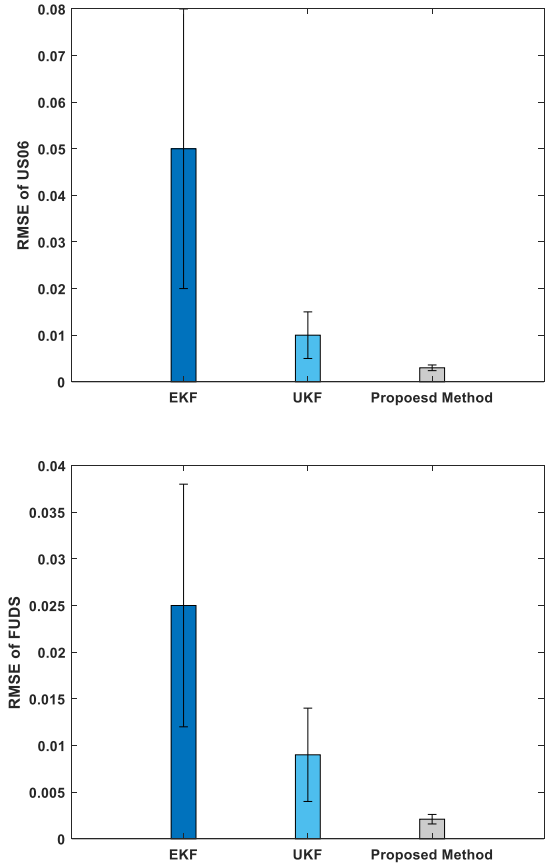

Fig.14. RMSE under unknown noise statistics

Finally, the effectiveness of the proposed method is assessed under non-Gaussian noise conditions. In this evaluation, the measurement noise is modeled using a Gamma distribution, while the process noise is assumed to follow a Gaussian distribution. Although the proposed method is theoretically formulated under Gaussian noise assumptions, it demonstrates strong resilience to non-Gaussian disturbances due to its adaptive structure. By leveraging real-time innovation statistics and an ANFIS-based adjustment mechanism, the filter dynamically updates the noise covariance matrices (Q_k and R_k), thereby accommodating variations such as skewness, heavy tails, or time-dependent noise profiles. This adaptive tuning enables the filter to maintain reliable performance without requiring explicit modeling of the noise distribution. The results, depicted in Fig.15, demonstrate that the proposed method outperforms both the EKF and UKF. For the EKF and UKF, the presence of non-Gaussian noise significantly impacts estimation accuracy, as these methods inherently rely on the assumption of Gaussian noise. In contrast, the proposed approach does not impose such a constraint, making it inherently more robust to variations in noise characteristics. This adaptability enhances its reliability in real-world applications, where noise distributions are often unknown or deviate from the Gaussian assumption.

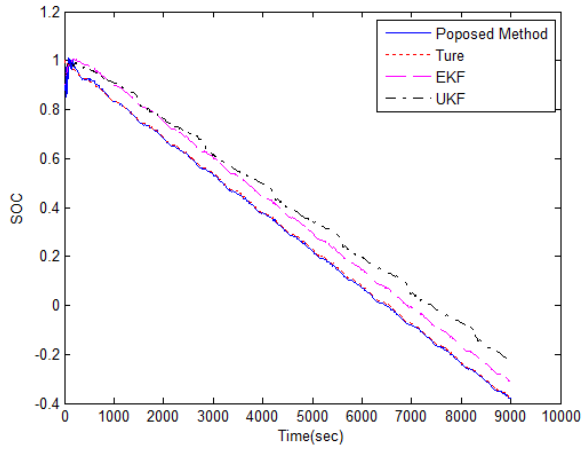

Fig.15 SOC estimation for US06 testing at 0 C

In a 10-cell configuration, each ARSRUKF estimator transmits state vectors (SOC, U_1, U_2) and Cholesky covariance factors at a nominal 100 Hz rate, resulting in a total data rate of 36 KB/s. ANFIS dynamically adjusts synchronization frequency to 10–200 Hz based on load dynamics, balancing accuracy and bus utilization. This approach ensures compatibility with automotive-grade CAN-FD networks (8 Mbps bandwidth), avoiding arbitration delays through prioritized alarm signaling.

VI. Conclusion

In this paper, we propose an advanced adaptive robust SR-UKF integrated with RLS for SOC estimation. The primary goal of this approach is to improve the robustness and accuracy of SOC estimation in the presence of uncertainties, especially when the statistical characteristics of process and measurement noise are unknown or variable. A key advantage of the proposed method is that it does not rely on prior knowledge of noise statistics, which are typically required in conventional filtering methods. Instead, covariance matrices for both process and measurement noise are dynamically adjusted in real-time using ANFIS. By combining the strengths of neural networks and fuzzy logic, ANFIS estimates optimal tuning parameters, enabling the filter to adaptively improve performance under varying operational conditions and environmental factors such as temperature changes and battery aging. The use of ANFIS allows effective modeling of nonlinear relationships and better handling of system uncertainties. By continuously adapting noise covariance parameters, the proposed method maintains high accuracy and stability even when noise characteristics are unknown or change over time. This makes the approach especially suitable for practical applications where accurate SOC estimation is critical, including EVs, renewable energy systems, and portable electronics. Experimental results demonstrate that the proposed SR-UKF

with RLS and ANFIS-based tuning significantly outperforms traditional methods in both accuracy and robustness. Notably, the proposed method provides more precise SOC estimates under challenging scenarios involving high noise levels, battery behavior variations, and unknown environmental influences. The proposed SR-UKF with RLS offers a promising solution for SOC estimation in systems with uncertain noise statistics. Its adaptability and inherent robustness make it a valuable tool for reliable SOC estimation in real-world applications. Future work could focus on further refining the method and exploring its performance in other complex scenarios. Scaling the framework to multi-cell battery packs introduces challenges such as cell-to-cell variability, balancing operations, and communication overhead. To address these, parallel ARSRUKF filters can be deployed at the cell level for individualized state estimation. Balancing-induced transient currents can be compensated by integrating current compensation techniques or coupling the estimators with balancing control algorithms. Efficient communication and synchronization between estimators are crucial, and distributed filtering architectures may provide scalable solutions for large battery systems. Furthermore, as part of our future work, we plan to perform real-time Hardware-in-the-Loop (HIL) validation of the proposed method. Preliminary hardware specifications for the HIL platform include a Texas Instruments TMS320F28379D dual-core DSP or an equivalent ARM Cortex-M7 microcontroller (e.g., STM32H7 series), with a minimum clock speed of 200 MHz. The system will support real-time sampling at 100 Hz to accommodate battery dynamics and ANFIS-based adaptive filtering. Sensor inputs will include voltage, current, and temperature measurements acquired via high-precision ADCs. The HIL test bench will replicate real-world load profiles (e.g., US06, FUDS) using programmable power supplies and battery emulators. These efforts aim to evaluate the algorithm's robustness and computational feasibility in embedded platforms.

References

[1] Q. Ouyang, J. Chen, and J. Zheng, "State-of-charging observer design for batteries with online model parameter identification: A robust approach," IEEE Transactions on Power Electronics, vol. 35, no. 6, pp. 5820–5831, Jun.2020.

[2] G.Mohebalizadeh, H.Alipour,L.Mohammadian, M.Sabahi, "An Improved Sliding Mode Controller for DC/DC Boost Converters Used in EV Battery Chargers with Robustness against the Input Voltage Variations", International Journal of Industrial Electronics, Control and Optimization,vol.4, no.2, pp.257-266 , 2021.

[3] G. Mohebalizadeh, H. Alipour, L. Mohammadian, and M. Sabahi, "An Improved Sliding Mode Controller for DC/DC Boost Converters Used in EV Battery Chargers with Robustness Against Input Voltage Variations," Int. J. Ind. Electron. Control Optim., vol. 4, no. 2, pp. 257–266, 2021.

[4] W. Waag, C. Fleischer, and D. U. Sauer, "Critical review of the methods for monitoring of lithium-ion batteries in electric and hybrid vehicles," Journal of Power Sources, vol. 258, pp. 321-339, Mar. 2014

[5] Y. Yang, Z. Tan, and Y. Ren, "Research on factors that influence the fast charging behavior of private battery electric vehicles," Sustainability, vol. 12, no. 9, p. 3439, Sep. 2020.

[6] F. Wang, Z. Zhai, B. Liu, S. Zheng, Z. Zhao, and X. Chen, "Open access dataset, code library and benchmarking deep learning approaches for state-of-health estimation of lithium-ion batteries," Journal of Energy Storage, vol. 77, Article 109884, 2024, doi: 10.1016/j.est.2023.109884.

[7] E. D. Silva-Vera, J. E. Valdez-Resendiz, G. Escobar, D. Guillen, J. C. Rosas-Caro, and J. M. Sosa, ''Data-driven modeling and open-circuit voltage estimation of lithium-ion batteries,'' Mathematics, vol. 12, no. 18, p. 2880, 2024.

[8] W. Bao, H. Liu, Y. Sun, and Y. Zheng, ''A fast prediction of open-circuit voltage and a capacity estimation method of a lithium-ion battery based on a BP neural network,'' Batteries, vol. 8, no. 12, p. 289, Dec. 2022.

[9] Q. Shi, Z. Jiang, Z. Wang, X. Shao, and L. He, "State of charge estimation by joint approach with model-based and data-driven algorithm for lithium-ion battery," IEEE Transactions on Instrumentation and Measurement, vol. 71, pp. 1–10, 2022.

[10] U. Westerhoff, T. Kroker, K. Kurbach, and M. Kurrat, ''Electrochemical impedance spectroscopy based estimation of the state of charge of lithiumion batteries,'' J. Energy Storage, vol. 8, pp. 244–256, . 2016.

[11] S. Su, W. Li, J. Mou, A. Garg, L. Gao, and J. Liu, "A hybrid battery equivalent circuit model, deep learning, and transfer learning for battery state monitoring," IEEE Transactions on Transportation Electrification, vol. 9, no. 1, pp. 1113–1127, Mar. 2023.

[12] F. Wang, Z. Zhai, B. Liu, S. Zheng, Z. Zhao, and X. Chen, "Open access dataset, code library and benchmarking deep learning approaches for state-of-health estimation of lithium-ion batteries," J. Energy Storage, vol. 77, p. 108529, Apr. 2024.

[13] Z. Chen, Y. Fu, and C. C. Mi, ''State of charge estimation of lithium-ion batteries in electric drive vehicles using extended Kalman filtering,'' IEEE

Trans. Veh. Technol., vol. 62, no. 3, pp. 1020–1030, Mar. 2013.

[14] J. Kim and B. H. Cho, "State-of-charge estimation and state-of-health prediction of a li-ion degraded battery based on an EKF combined with a per-unit system," IEEE Trans. Veh. Technol., vol. 60, pp. 4249-4260, 2011.

[15] Y. Tian, B. Xia, W. Sun, Z. Xu, and W. Zheng, ‘‘A modified model based state of charge estimation of power lithium-ion batteries using unscented Kalman filter,’’ J. Power Sources, vol. 270, pp. 619–626, Dec. 2014.

[16] Wang Qiuting, Lu Yunhao, JY, “State of health estimation for lithium-ion battery based on D-UKF”, Int. J. Hybrid Inf. Technol., vol.8, no.16, 2015.

[17] J. Ma, Y. Hu, Q. Ma, S. Yang, J. Zheng, and S. Wang, ‘‘Improved adaptive filter with unknown process and measurement noise covariance,’’ in Proc. Chinese Intell. Syst. Conf., 2020, pp. 792–800.

[19] B. Gao, S. Gao, G. Hu, Y. Zhong, and C. Gu, ‘‘Maximum likelihood principle and moving horizon estimation based adaptive unscented Kalman filter,’’ Aerospace Sci. Technol., vol. 73, pp. 184–196, Nov. 2024.

[18] J. Meng, G. Luo, and F. Gao, ‘‘Lithium polymer battery state-of-charge estimation based on adaptive unscented Kalman filter and support vector machine,’’ IEEE Trans. Power Electron., vol. 31, no. 3, pp. 2226–2238,Mar. 2016.

[19] M. Partovibakhsh and G. Liu, “An Adaptive Unscented Kalman Filtering Approach for Online Estimation of Model Parameters and State-of-Charge of Lithium-Ion Batteries for Autonomous Mobile Robots,” IEEE Trans. Control Syst. Technol., vol. 23, no. 1, pp. 357-363, 2015.

[20] Q. Shi, Z. Jiang, Z. Wang, X. Shao, and L. He, "State of charge estimation by joint approach with model-based and data-driven algorithm for lithium-ion battery," IEEE Transactions on Instrumentation and Measurement, vol. 71, pp. 1–10, 2022.

[21] S. Su, W. Li, J. Mou, A. Garg, L. Gao, and J. Liu, "A hybrid battery equivalent circuit model, deep learning, and transfer learning for battery state monitoring," IEEE Transactions on Transportation Electrification, vol. 9, no. 1, pp. 1113–1127, Mar. 2023.

[22] J. Meng et al., “An Overview and Comparison of Online Implementable SOC Estimation Methods for Lithium-Ion Battery,” in IEEE Transactions on Industry Applications, 2018, vol. 54, no. 2, pp. 1583–1591.

[23] R. Xiong, J. Cao, Q. Yu, H. He, and F. Sun, “Critical Review on the Battery State of Charge Estimation Methods for Electric Vehicles,”IEEE Access, vol. 6, pp. 1832–1843, 2018.

[24] Jinhao Meng, Daniel-Ioan Stroe, Mattia Ricco, “A Simplified Model based State-of-Charge Estimation Approach for Lithium-ion Battery with Dynamic Linear Model”, IEEE Transactions on Industrial Electronics,vol.66,no.10,2018.

[25] Zhuang, Y., Wang, Z., Yu , H., Wang, W. , Lauria , S. “A robust extended H∞ filtering approach to multi-robot cooperative localization in dynamic indoor environments”, Control Engineering Practice ,vol.21, pp.953–961, 2013.

[27] P. Zhang, W. Wang, M. Gao, and Y. Wang, ‘‘Square-root cubature Kalman filter based on H∞ filter for attitude measurement of high-spinning aircraft,’’ Int. J. Aerosp. Eng., vol. 2021, Article ID 5589691, May 2021.

[26] T. Q. Duong, “USABC and PNGV test procedures,” Journal of Power Sources, vol. 89, no. 2, pp. 244–248, 2000.

[27] W. He, N. Williard, C. C. Chen, and M. Pecht, “Robust and adaptive estimation of state of charge for lithium-ion batteries,” International Journal of Power Electronics, vol. 62, pp. 783–791, 2014.

[28] Z. Ma, J. Jiang, W. Shi, W. Zhang, and C. C. Mi, “Investigation of path dependence in commercial lithium-ion cells for pure electric bus applications: aging mechanism identifcation,” Journal of Power Sources, vol. 274, pp. 29–40, 2015.

Ramazan Havangi received his M.S. and Ph.D. degrees from the K.N. Toosi University of Technology, Tehran, Iran, in 2003 and 2012, respectively. He is currently an Associate Professor of control systems with the Department of Electrical and Computer Engineering, University of Birjand, Birjand, Iran. His main research interests are inertial navigation, integrated navigation, estimation and filtering, evolutionary filtering, simultaneous localization and mapping, fuzzy, neural network, and soft computing.

Fatemeh Karimi was born in Borujerd, Iran. She received her associate degree in telecommunications, her B.Sc. degree in electronics engineering, and her M.Sc. degree in control engineering all from Islamic Azad University in 2003, 2008, and 2013, respectively. She is currently a Ph.D. candidate of control engineering at the state-run University of Birjand. Her research interests include function fields, active power filters, multi-agents, and Kalman filters.